

The Influence of Thermal Diffusion on Laser Ablation of Metal Films

E. Matthias¹, M. Reichling¹, J. Siegel¹, O. W. Käding¹, S. Petzoldt¹, H. Skurk¹, P. Bizenberger², E. Neske²

¹ Fachbereich Physik, Freie Universität Berlin, Arnimallee 14, D-14195 Berlin, Germany (Fax: +49-30/8386059)

² Fraunhofer-Institut für Physikalische Meßtechnik, Heidenhofstrasse 8, D-79110 Freiburg i. Br., Germany (Fax: +49-761/8857224)

Received 30 August 1993/Accepted 9 October 1993

Abstract. Single-shot ablation thresholds of nickel and gold films in the thickness range from 50 nm to 7 μm have been measured for 14 ns laser pulses at 248 nm, using photoacoustic shock wave detection in air. The metal films were deposited on fused silica substrates. The ablation threshold was found to increase linearly with film thickness up to the thermal diffusion length of the film. Beyond this point it remains independent of film thickness. The proportionality between threshold fluence and thickness allows the prediction of ablation thresholds of metal films from the knowledge of their optical properties, evaporation enthalpies and thermal diffusivities. Physically it proves that ablation is driven by the energy density determined by the thermal diffusion length. A simple thermodynamic model describes the data well. Thermal diffusivities, an essential input for this model, were measured using the technique of transient thermal gratings. In addition, the substrate dependence of the ablation threshold was investigated for 150 nm Ni films.

PACS: 68.60.Dv, 79.20.Ds

When thermal processes like melting and evaporation govern laser ablation, the question arises whether single-shot threshold fluences can be predicted by optical and thermal properties of the material. This problem has been discussed ever since laser ablation of materials gained greater interest [1–5]. However, to our knowledge, there is still no model which reliably describes the *onset of ablation* for any material in terms of its optical and thermal attributes. Usually the threshold fluence is treated as a parameter to fit the experimental data.

In the past, much effort has been spent on laser ablation of *polymers*, and most of the relevant literature up to 1991 was listed by Babu et al. [6]. In a phenomenological approach, these authors used a superposition of photothermal and photochemical effects to describe their observed etch rates. Brannon et al. [7] and Küper et al. [8] pointed out that for some polymers and wavelengths the ablation depth per pulse can be described by an Arrhenius-type rate law, indicating

a thermal process for which the temperature is assumed to be proportional to the laser fluence. A consequence of this is that there exists no sharp ablation threshold, instead, this is set by the detection sensitivity [8].

The role of thermal conductivities for laser damage of *optical materials* was reviewed by Guenther and McIver [9]. In this area, Decker et al. [10] were the first to emphasize the importance of thermal conductivity for the performance of optical coatings. These authors reported thermal conductivities for thin films of SiO_2 and Al_2O_3 two orders of magnitude smaller than bulk values, but made no quantitative prediction for correspondingly lower damage thresholds. This was first done by Ristau et al. [11] and Akhtar et al. [12], who established a correlation between thermal conductivity, optical absorption, and damage threshold, with the latter being defined by the melting temperature. Independently, Lange et al. [13] developed an “absorbing-inclusion model” and showed that laser damage in optical coatings depends on the thermal properties of the coating material. In their model, the threshold fluence for ablation, F_T , is proportional to the melting temperature, T_m , multiplied by the square root of laser pulse length, τ_L , and the material constants: density, ρ , specific heat at constant pressure, c_p , and thermal conductivity, K . The success of this formula was limited, mostly because the thermal conductivity may vary with film thickness. However, reports about measurements of both, thermal properties and damage thresholds of dielectric coatings remained sparse [14].

Laser melting and etching of *metals* and *metal films* has been investigated by many researchers and the main results are summarized in [1–4]. An important factor is the *reflectivity*, R , of the surface which, for thermal equilibrium [15], sensitively depends on the pretreatment of the sample and its amorphous or crystalline nature [16, 17]. Although the *thermal diffusivity*, κ , has been recognized as another key quantity in laser melting, little effort seems to have been spent to actually studying it in connection with laser ablation of metal films. In fact, we are only aware of the work by Andrew et al. [18] who measured the thickness dependence of threshold fluences, required to remove with a single laser shot Al films on glass and Ag films on mylar. These authors

also reported single-shot ablation thresholds at 308 nm for other metal films of around 100 nm thickness on different substrates. They calculated the temperature rise of the metal films and found that in all cases the so called “removal threshold” was significantly smaller than the fluence required for vaporization and more in agreement with the melting threshold.

In this contribution we present results about single-shot damage thresholds and thermal diffusivities of Ni and Au films of varying thicknesses on fused silica substrates. Fused silica was selected as substrate material because of its poor thermal conductance. Hence, during the laser pulse the heat piles up in the film, leading above a certain fluence threshold to melting and, at still higher fluences, to evaporation. By varying the film thickness, d , we show that the *thermal diffusion length*,

$$L_{th} = (2\kappa\tau_L)^{1/2}, \quad (1)$$

governs the fluence thresholds for melting or vaporization. Note that we use here the length where the temperature is only reduced by $e^{-1/2}$. For thicknesses $d \leq L_{th}$, we find that the ablation threshold increases linearly with film thickness. Once the metal film is thicker than L_{th} , the fluence required for melting or ablation is independent of thickness. This behavior can be understood by a simple thermal model. It is based on the fact that, in the nanosecond pulse regime, the *critical energy density*, ε_T , required for melting or vaporization is given by $\varepsilon_T = F_T/L_{th}$. This is to be distinguished from the energy density $\varepsilon_\alpha = F_T\alpha$ in the volume determined by the optical absorption length $1/\alpha$ (see Fig. 1). In case of Ni, $1/\alpha$ is about 8 nm at a wavelength of 248 nm. With 14 ns laser pulses, this amounts to a ratio of $\varepsilon_\alpha/\varepsilon_T \approx 100$, indicating that only about 1% of the absorbed energy is effective in causing melting or evaporation at the surface. Consequently, when reducing the film thickness to a range $1/\alpha < d < L_{th}$, the threshold fluence will be reduced by the ratio d/L_{th} . The experiments reported below have been designed to prove this simple concept.

1 Experimental Techniques

1.1 Measurement of Ablation Thresholds

Single shot damage behavior of Ni and Au films was measured in air, using a 1-on-1 irradiation mode with 14 ns laser pulses of 248 nm wavelength. The laser beam had a good quality top hat profile. The two main parameters varied were laser fluence and thickness of the metal films. The films were sputter-deposited on fused silica substrates. While the Ni films stuck directly on the substrate, Au films needed an intermediate Cr film to adhere. In the experiments, two threshold fluences were recorded. One was the fluence where the irradiated spot became visible and could be recognized by optical microscopic inspection. We identify this visibility threshold with the beginning of surface melting. The other threshold at higher fluences could be detected by shockwave emission and signaled the onset of evaporation. It was monitored by means of the probe beam deflection technique, the principle of which is sketched in Fig. 1 and described elsewhere [19]. A rapidly expanding plasma generates a

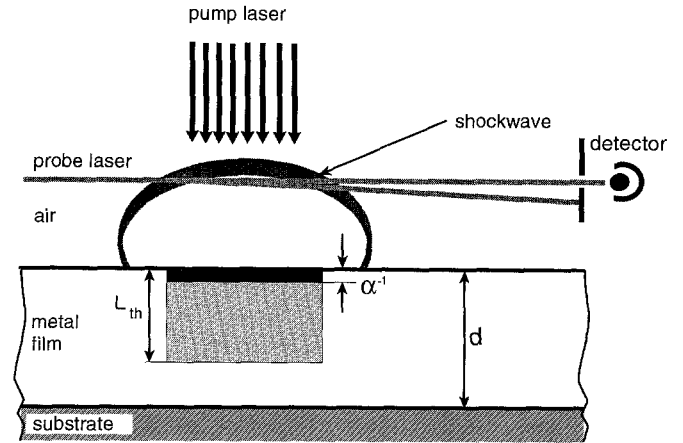


Fig. 1. Principle scheme for detecting acoustic pulses emitted from a target surface during pulsed laser irradiation. Sketched is a shockwave causing the deflection of a HeNe probe laser beam oriented parallel to the surface at a distance of a few millimeters. The optical absorption depth and the thermal diffusion length for nanosecond laser pulses are indicated

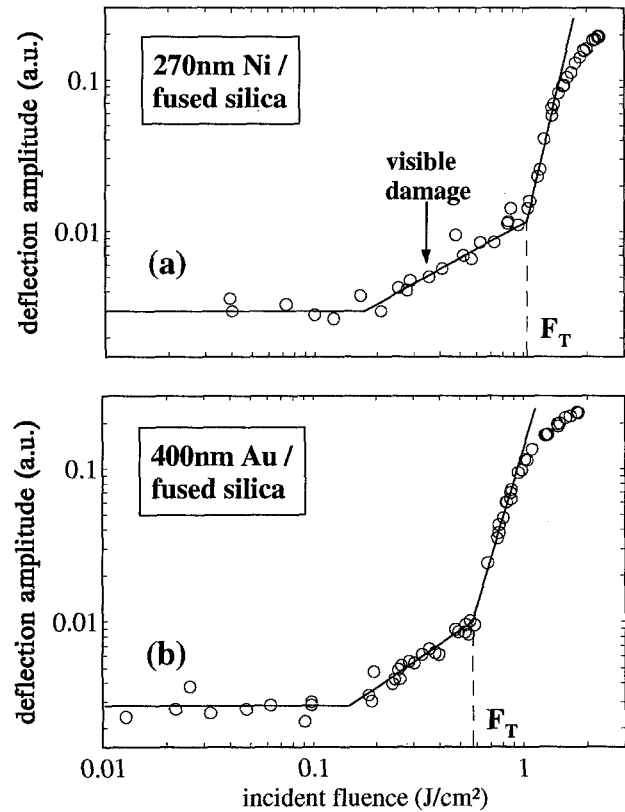


Fig. 2a, b. Typical fluence dependences of the probe beam deflection amplitude for (a) 270 nm Ni and (b) 400 nm Au films on fused silica. Each data point was recorded at a virgin surface spot (1-on-1 mode). The upper threshold is interpreted as damage threshold, F_T . The fluence above which the spots are visible in (a) is indicated by an arrow. *Solid lines* are drawn to guide the eye

shock front which causes a transient change in refractive index, that can be detected by the deflection of a probe beam which runs parallel to the surface at a distance of 3 mm.

In Fig. 2 the peak-to-peak amplitudes of the beam deflection signals are shown as a function of incident fluence for

270 nm Ni and 400 nm Au films. For all films we reproducibly observed two sharp bends in the data trend which we attributed to distinctly different effects. The lower bend is interpreted as the appearance of a photoacoustic signal caused by surface heating. The gas close to the irradiated spot expands and generates a sound wave which deflects the probe beam. Since there is no real threshold for heating, the break of the data slightly below 0.2 J/cm^2 indicates the fluence, above which the signal exceeds the noise level.

The bend of the data at higher fluence, marked by F_T , represents the onset of shockwave generation caused by evaporation and plasma formation. About half way between the two breaks in the data trend we found a threshold fluence at which the irradiated spot at the surface became visible by inspection with an optical microscope. This threshold is attributed to melting and will be used together with F_T for a more detailed analysis. At the highest measured fluences one can also recognize the decreasing slope of the data which indicates where the plasma becomes optically dense.

The interpretation given for the two breaks in the fluence dependence of the beam deflection amplitude in Fig. 2 was checked by measuring the transit time of the pressure wave between target surface and probe beam as a function of fluence. In Fig. 3 the results are displayed for two Ni films, differing in thickness by more than one order of magnitude.

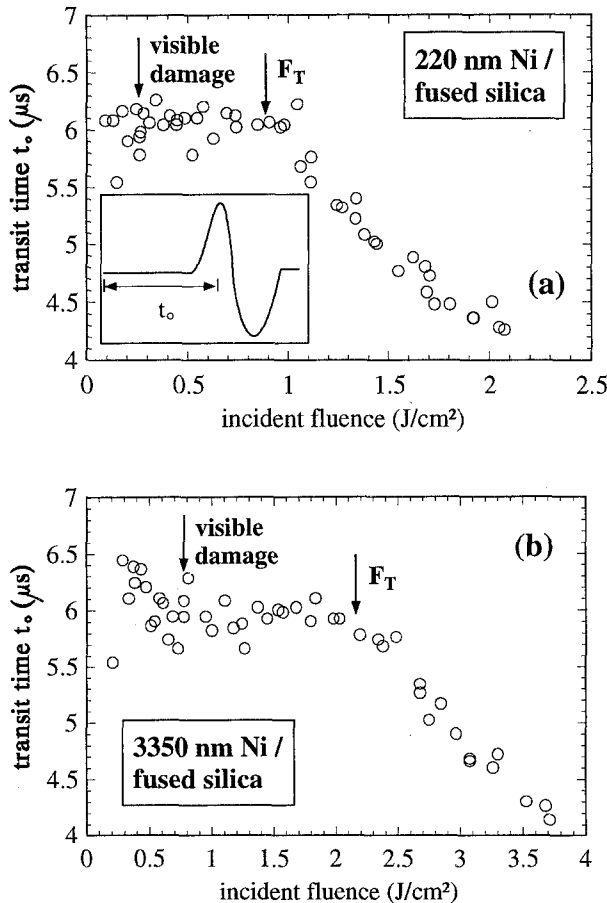


Fig. 3a, b. Transit time of the pressure wave between surface and probe beam as a function of fluence for two Ni films of different thickness. The break in slope at F_T indicates the onset of a supersonic pressure wave. The transit time is defined in the inset of (a)

The transit time is defined in the inset of Fig. 3a. This definition is chosen for convenient data analysis, and is not identical with the start of the deflection signal. The HeNe laser beam was unfocused ($\varnothing \approx 1.5 \text{ mm}$), and its center was at a distance of 3.0 mm from the surface. Despite the scatter of the data it is apparent that there exist two different fluence ranges for the transit time. Up to F_T , the transit time is independent of fluence. It corresponds to the speed of sound of the acoustic signal generated by surface heating. The constant transit time even holds at fluences where visible damage, i.e., melting occurs. The second fluence range is above the ablation threshold, F_T , where we observe a nonlinear decrease (Fig. 3a) of the transition time with increasing fluence. This behavior is typical for the motion of a shock front driven by the emission of supersonic particles. Note that the threshold fluences in Fig. 3 differ greatly for the two film thicknesses. They are consistent, however, with the values obtained from measurements of the shockwave amplitude, like the ones shown in Fig. 2. Hence, measurements of transit times provide an alternative way to determine ablation thresholds.

1.2 Measurements of Thermal Diffusivities

In parallel with the threshold fluence measurements, thermal diffusivities, κ , were measured for all Ni and Au films in order to control a possible variation with thickness. Further, this quantity provides a test for the quality of the metal films. There exist a sizable number of different techniques for measuring thermal conductivities [10–12, 20–23]. This provides the choice to select an optimal technique for a given task. For metal films on poor thermal conductors, the Transient Thermal Grating (TTG) technique [24] was considered to be most appropriate since it is sensitive to heat transport in the plane of the metal film [25]. The huge difference between bulk thermal diffusivities [26] of metals (Ni: $0.19 \text{ cm}^2/\text{s}$, Au: $1.29 \text{ cm}^2/\text{s}$) and fused silica ($0.0087 \text{ cm}^2/\text{s}$) implies that in metal films on quartz glass lateral heat diffusion plays a significant role whenever the films are thinner than L_{th} .

The principle of the TTG technique is sketched in Fig. 4. The pump laser is split into two beams which are reunited

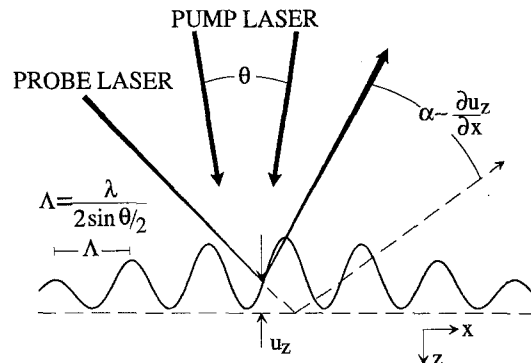


Fig. 4. Principle scheme of the Transient Thermal Grating (TTG) method for measuring thermal diffusivities. The grating, generated by a periodic thermal expansion of the surface can be detected by diffraction, thermorefectance, or displacement measurements. The latter detection technique is indicated.

in the surface plane, generating an interference pattern that translates into a temperature grating and a corresponding periodic surface deformation. The grating can be monitored by diffraction [27], by surface displacement [24, 25], or by thermoreflectance. In particular the latter technique records, for short time intervals following the laser pulse, predominantly the lateral heat flow when the reflectance is measured in the minima of the temperature grating. We have used both, thermoreflectance and displacement detection. Figure 4 illustrates the displacement technique which traces the grating by the change in reflection angle of a probe beam and measures the derivative of the grating pattern. The lateral thermal diffusivity can be inferred from the decay of the displacement grating. In case of a homogeneous material the decay is exponential, with a decay rate [27]

$$\tau^{-1} = \kappa(2\pi/\Lambda)^2 \quad (2)$$

where $(2\pi/\Lambda)$ is the grating vector. By varying the grating period Λ , the thermally active volume can be controlled: the smaller the lateral dimension Λ , the smaller is the vertical

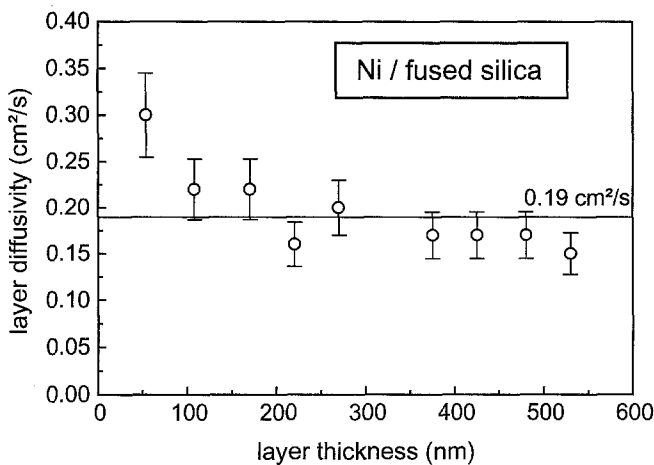


Fig. 5. Thermal diffusivities of Ni films on fused silica as a function of thickness. The values have been measured by the displacement technique and are corrected for substrate contributions by using a complete analysis. The mean value of all thicknesses is indicated

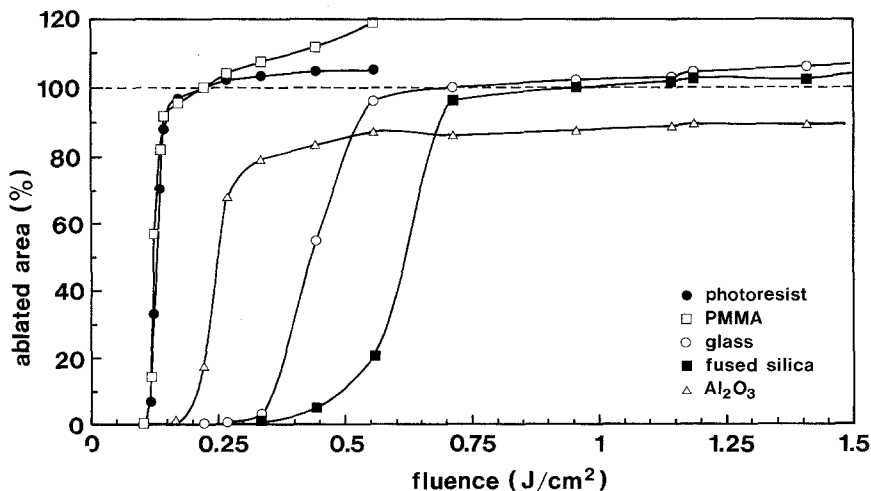


Fig. 6. Single-shot ablation behavior of 150 nm Ni films on various substrate materials. Plotted is the percentage of ablated to irradiated area as a function of fluence

penetration depth of the heat. Consequently, the asymptotic limit of small Λ is most sensitive to the heat flow near the surface, which implies for a film/substrate system that it measures the thermal diffusivity of the film. This simple type of analysis has proved very useful for quickly characterizing thermal properties of thin films and also checking the quality of the measurements. An accurate description of the grating decay requires a more comprehensive treatment based on a three-dimensional thermoelastic theory for the complete film/substrate system [28]. As mentioned before, the grating pattern was also detected by the periodic change of the thermoreflectance, which tests the temperature directly. Such type of measurements avoid the difficulty of describing the thermoelastic coupling correctly, and are useful for obtaining a consistency check of the displacement data [28].

Figure 5 displays the results of thermal diffusivity measurements on Ni films of different thicknesses up to 540 nm, obtained by the displacement technique. The decay rates were analyzed by numerically solving the complete theoretical model for the film/substrate system and correcting the film diffusivities for substrate contributions. Within their errors, these data show no significant variation with thickness. We believe that this is typical for high quality metal films on thermally insulating substrates. Hence, we can use a constant value of the thermal diffusion length for the analysis of the ablation threshold data and need not consider any thickness dependence of κ . By averaging the data in Fig. 5 a thermal diffusivity of $(0.19 \pm 0.02) \text{ cm}^2 \text{ s}^{-1}$ is obtained for Ni-films, in excellent agreement with the bulk value for Ni [26].

Displacement and thermoreflectance measurements were also carried out on Au films. The results scattered significantly more than the ones for Ni films in Fig. 5. The reason is probably a 50 nm intermediate Cr layer which was used in all cases to ensure adhesion of Au films on fused silica. The scatter of the Au data showed no trend with film thickness. We found an average value of $\kappa(\text{Au}) = 0.39 \text{ cm}^2 \text{ s}^{-1}$ to be used for the data analysis in Sect. 2.2. Note that this number amounts to only about 1/3 of the Au bulk value and is much closer to the one for Cr bulk ($0.30 \text{ cm}^2 \text{ s}^{-1}$), supporting the suspicion that the Cr intermediate layer badly distorts the thermal diffusion data of the Au films.

1.3 Influence of Substrate Materials on Ablation Thresholds

In principle, ablation thresholds of thin metal films should depend on the thermal properties of the substrate. Since this question is of great importance for technological applications, we investigated, as an example, the percentage ablation for single shot irradiation of 150 nm Ni films on various substrates. The results are shown in Fig. 6. Plotted is the ratio of ablated to irradiated area as a function of incident fluence. We notice a strong influence of the substrate on the ablation characteristics. On the other hand, there is no obvious correlation between the thermal diffusivity of the substrate and either the onset of ablation or the fluence at which the irradiated area is completely removed. We suspect that the reason lies in the attachment of the film to the substrate. The unknown thermal resistance of the interface is most likely quite different for the various substrates, and must be known for a satisfying analysis of the data in Fig. 6. To our knowledge, this question has not been systematically investigated, but is beyond the scope of our present paper.

2 Results and Discussion

2.1 Critical Energy Densities for Melting and Evaporation

Fluence dependencies of the deflection amplitude, as displayed in Fig. 2, have been measured for Ni and Au films of different thicknesses. For each film the ablation threshold, F_T , and the threshold for visible damage were determined. These values are plotted as a function of thickness in Fig. 7 for Ni and in Fig. 8 for Au. In both cases we find a similar systematics, characterized by a conspicuous break of the data trend at a specific thickness. For thin films the thresholds increase linearly with thickness up to a value given by the thermal diffusion length. For thicknesses above L_{th} , both threshold fluences remain approximately constant. The constant slope, $\varepsilon_T = F_T/L_{th}$, of the data in the range of linear increase proves that a critical energy density ε_T exists, which must be exceeded to achieve damage. On the basis of the data in Figs. 7 and 8, we propose that this quantity is a specific property for each film material, provided the substrates are poor thermal conductors. Consequently, in the range $d \leq L_{th}$, where L_{th} is to be substituted by the film thickness d , the threshold fluence F_T will be reduced accordingly. As discussed before, the physical reason for this result is that for good thermal conductors the heat spreads in one nanosecond over a distance of a few hundred nanometers, i.e., into a volume composed of irradiated area times thermal diffusion length. In case $d \leq L_{th}$, the film thickness will be the limiting depth as long as the substrate is a poor thermal conductor. This means that from the totally absorbed energy, only the fraction $(\alpha d)^{-1}$ is contributing to surface melting or ablation. For applications, it will be of importance that this fraction can be manipulated by the proper choice of pulse length and film thickness. These conclusions can be tested by measuring single-shot ablation contours of nickel films on insulating substrates. Good precision is expected only for thicknesses smaller than the thermal diffusion length, L_{th} . This is illustrated in Fig. 9, where electron microscopy

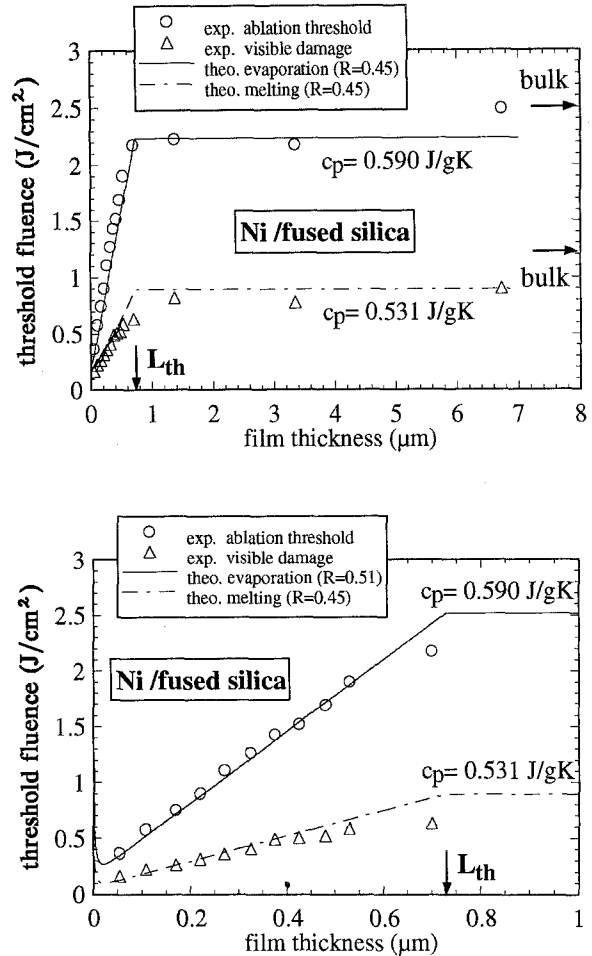


Fig. 7. Thickness dependence of single shot threshold fluences for visible damage (triangles) and ablation (circles) of Ni films on fused silica, obtained from measurements like the one shown in Fig. 2a. The lower frame is an expanded version of the upper picture up to 1 μm thickness. The solid and dashed-dotted lines are calculated by (6) and (7) in Sect. 2.2. Note that in the lower picture the reflectivity of the molten phase was assumed to be about 10% higher than for the solid surface

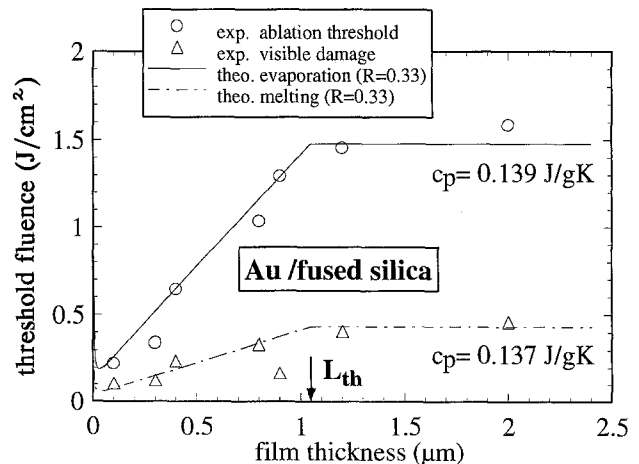


Fig. 8. Thickness dependence of single-shot threshold fluences for visible damage (triangles) and ablation (circles) for Au films on fused silica, taken from measurements like the one shown in Fig. 2b. The reflectivity of the molten and solid phase was assumed to be equal

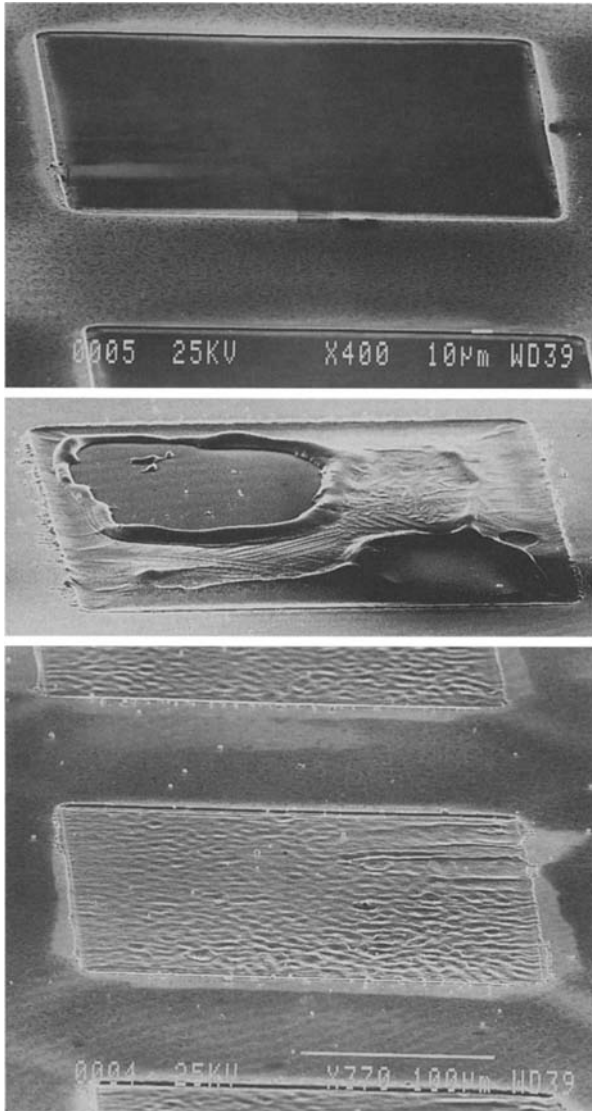


Fig. 9. Electron microscopy images of three Ni films irradiated with a single 14 ns, 248 nm laser pulse at an incident fluence of 4 J/cm^2 . The respective thicknesses are: 440 nm (*upper*), 960 nm (*middle*), and $3.7 \mu\text{m}$ (*lower*). In comparison, the thermal diffusion length is $L_{\text{th}} \approx 0.73 \mu\text{m}$

Table 1. Comparison of experimentally observed energy densities and literature values of enthalpies for nickel and gold films in kJ/cm^3

	Ni: Visible damage (melting)	Ni: Ablation threshold (evaporation)	Au: Visible damage (melting)	Au: Ablation threshold (evaporation)
Experiment	4.3 ± 0.2	16.0 ± 0.8	2.2 ± 0.5	8.8 ± 1.4
Literature	7.19	18.39	2.86	9.25

images show the ablated areas on Ni films of different thicknesses. The ablation patterns correspond to the rectangular cross section of the laser beam used in this case. As shown in the upper picture, for a film with $d = 440 \text{ nm} < L_{\text{th}}$, a comparably clean ablation is obtained with a single laser shot of fluence of 4 J/cm^2 . In contrast, the middle picture shows the ablation result with the same fluence for a film of thickness $d = 960 \text{ nm} > L_{\text{th}}$. The whole irradiated area was molten

but only parts of it are evaporated. Clearly, such outcome is unacceptable for any application purpose. Finally, the lower frame shows the result for a 3700 nm thick film. In view of these pictures it must be remembered, that 4 J/cm^2 is a very large fluence, already in the range where the plasma strongly absorbs the radiation (cf. Fig. 2).

The energy densities obtained from a fit to the linear slopes in Figs. 7 and 8 and corrected for reflectivity loss are listed in Table 1. When comparing these experimental results with melting and evaporation enthalpies of bulk Ni and Au, we find surprisingly good agreement. The general trend is that the experimental values are systematically smaller than the literature bulk values. This reflects the energy loss to the substrate. The larger difference for Ni suggests that the adhesion of Ni films to the substrate was better and allowed a better heat transfer to the quartz glass compared to the situation for Au films. A question in this context is the influence of oxide layers on the ablation threshold. We believe, however, that it is of no importance and will not affect the values in Table 1. The important result is that the agreement is sufficiently good to allow a reasonable prediction of the ablation threshold from the knowledge of reflectivity, evaporation enthalpy and thermal diffusion length.

2.2 Thermodynamic Model

In order to describe the thickness dependence of the threshold fluences, shown in Figs. 7 and 8, we assume a purely thermal origin of the observed threshold effects. We identify the visibility threshold with the melting point and the ablation threshold with the onset of evaporation. Lateral heat diffusion can be neglected because of the large diameter ($500 \mu\text{m}$) of the irradiated spot. Furthermore, we ignore heat loss to the gas layer near the surface. The fact that the heat has spread within 14 ns nanoseconds to a depth given by the diffusion length, allows us to assume a uniform temperature rise

$$\Delta T = \Delta Q / C_p \quad (3)$$

throughout this volume. Here, ΔQ is the totally absorbed energy and C_p the heat capacity at constant pressure. We introduce the specific heat, c , and define a thermally active depth, ℓ_f , for the film, which is

$$\ell_f = d \quad \text{for } d < L_{\text{th},f}, \quad (4)$$

and

$$\ell_f = L_{\text{th},f} \quad \text{for } d \geq L_{\text{th},f}. \quad (5)$$

The subscript f denotes film quantities. When $d < L_{\text{th},f}$, we include heat loss to the substrate and introduce the thermal diffusion length, $L_{\text{th},s}$, of the substrate. This is additively taken into account, neglecting any thermal resistance at the interface between film and substrate. Inserting the proper expression for the absorbed energy, the *threshold fluence for melting* can be expressed in the form

$$F_{\text{Tm}} = \frac{\Delta T_m}{(1 - e^{-\alpha d})(1 - R)} \times \left\{ \left[\rho_f c_f - \left(\frac{L_{\text{th},s}}{L_{\text{th},f}} \right) \rho_s c_s \right] \ell_f + L_{\text{th},s} \rho_s c_s \right\}. \quad (6)$$

Here R is the reflectivity of the surface, and ΔT_m is the temperature increase needed for melting. Recalling (4), this equation describes the observed linear dependence on film thickness, up to the point where d is equal to the thermal diffusion length. Then (5) has to be inserted into (6) with the result that the terms containing substrate quantities cancel and the last bracket reduces to the materials constant ($\rho_f c_f L_{th,f}$). Since $\exp(-\alpha d)$ becomes important only for very small thicknesses, the reflectivity, R , and the thermal diffusion length of the film, $L_{th,f}$, are the crucial quantities when evaluating the threshold fluence from the material properties of the film.

The dashed-dotted lines in Figs. 7 and 8 are *no fit* to the data (triangles) but represent the fluence dependence predicted by (6). The values used for the specific heat and the reflectivity are given in the figures. Since the specific heat varies linearly with temperature in the range considered here, its temperature dependence was taken into account by using the average value between room temperature and the respective melting or evaporation point [29]. With the thermal diffusivities given in Sect. 1.2 for Ni and Au, and a laser pulse width of 14 ns we obtain from (1) $L_{th}(\text{Ni}) = 0.73 \mu\text{m}$ and $L_{th}(\text{Au}) = 1.05 \mu\text{m}$. Taking the melting temperature from the tables [29] and inserting these values into (6), we find for both, Ni and Au, good agreement with the measured threshold fluence for melting. This is quite surprising since we identified the melting threshold in a rather subjective manner by the appearance of a visible spot.

The onset of ablation, measured by the beam deflection method discussed in Sect. 1.1 represents a more accurate result. Its fluence dependence on thickness should obey the same formalism as outlined above, as long as the melting temperature is substituted by the sum of the temperature rise for evaporation, ΔT_v , and the latent heat for melting, ΔH_m , divided by the specific heat:

$$\Delta T_m \rightarrow \Delta T_v + \Delta H_m / \rho_f c_f. \quad (7)$$

Using the same material constants as before and taking ΔT_v and ΔH_m from the tables, this simple model describes the ablation data in Figs. 7 and 8 (circles) very well, as evidenced by the solid lines. These are no fit to the data but calculated using (6), with the melting temperature substituted according to instruction (7). The Ni data scatter much less and are, therefore, more reliable compared to the ones for Au. However, remembering that the Au-films were coated onto an intermediate chromium layer, it is surprising that the model fits the Au-data as well. After all, the thermal diffusivity of the Au films was about a factor of 3 smaller than the bulk value.

Notice in the lower frame of Fig. 7 that the reflectivity of Ni was changed from $R = 0.45$ to $R = 0.51$ when going from the solid to the liquid surface in order to approach the experimental results even better than in the upper frame, where only one value of the reflectivity was used. At this stage we have no data to elaborate further on this point. It should only serve to emphasize that the reflectivity change during the laser pulse deserves more attention, in particular for thin-film materials.

The astounding agreement between experimental data and the prediction by (6) and (7) of the ablation threshold for

both Ni and Au films proves that the ansatz of our simple model is basically correct, and that dynamic processes play no role on the nanosecond time scale. Also, the ablation threshold does not seem to be sensitive to the thermal resistance of the interface, which we neglected. In the range $\alpha^{-1} < d < L_{th}$ the ablation threshold indeed varies linearly with thickness, confirming the empirical knowledge that thin films are destroyed at lower fluences than thicker ones. For very small thicknesses the influence of α can be noticed in the theoretical curves in Figs. 7 and 8. The prediction is that in this range the fluence should rise again steeply, which might be worthwhile testing.

3 Conclusion

In summary, an investigation of the thickness dependence of fluence thresholds for melting and evaporation has been carried out for Ni and Au films on fused silica substrates. The important point of this work was the systematical variation of the thickness of the metal films below the thermal diffusion length. Experimentally, we find a linear dependence of both thresholds on thickness, d , as long as d is larger than the optical absorption depth, α^{-1} , and smaller than the thermal diffusion length, L_{th} , of the film. For thicknesses larger than L_{th} , the thresholds are independent of thickness. This result shows that for the onset of damage, a critical energy density is required which is determined by fluence divided by the thermal diffusion length (F_T/L_{th}). Hence, during nanosecond pulses, the initially deposited energy density ($F_T \alpha$) dissipates rapidly into a (αL_{th})-larger volume and contributes only with the inverse fraction of it to the damage of the surface layer.

One consequence of this is that clean single-shot ablation can only be obtained for thicknesses smaller than the diffusion length (cf. Fig. 9). On the other hand, in order to achieve a high damage resistance, for example for metallic masks, film thicknesses equal or larger than the thermal diffusion length are required.

From the slopes of the linear dependence, the critical energy densities required for accomplishing damage are obtained. They are in reasonable agreement with the tabulated bulk enthalpies for melting and evaporation, but consistently somewhat lower due to heat loss to the substrate. An important consequence of these findings is that for metal films on thermally poor conducting substrates, ablation thresholds can be approximately predicted from the reflectivity, thermal diffusion length, and the evaporation enthalpy of the material.

A model based on simple thermodynamical assumptions was developed to understand the observed linear relationship between the threshold fluences and film thickness. Without the need for any free parameters and based on material constants only, the model describes the experimental data well and allows the prediction of damage thresholds from these constants. It also emphasizes the importance of both, thermal diffusion length and optical reflectivity of the film for predicting melting and ablation thresholds. Since these quantities may be different for thin films compared to bulk values, it is necessary to check them in each individual

case. For this reason, thermal diffusivities were measured for Ni and Au films by means of the transient thermal grating technique. As a result, we find that our Ni films show no variation of thermal diffusivity with thickness and are well characterized by the bulk value. In case of Au films, which were deposited on a Cr intermediate layer, the data scattered more and the average came out as low as 1/3 of the bulk value. This Au–Cr double layer on fused silica behaved optically like gold and thermally like chromium.

In another set of measurements, the ablation efficiency of 150 nm Ni films on various substrate materials was studied. No unambiguous correlation was found between the ablation behavior and the thermal diffusivity of the substrates. Most likely, adhesion quality and thermal contact to the substrate obscures such correlation in the investigated cases, and should be known in detail in order to understand the experimental data.

Acknowledgement. This project was supported by the BMFT/VDI-Verbundprojekt 13N 5627.

References

1. R.M. Wood: *Laser Damage in Optical Materials* (Adam Hilger, Bristol 1986)
2. M. von Allmen: *Laser-Beam Interactions with Materials*, Springer Ser. Mater. Sci., Vol. 2 (Springer, Berlin, Heidelberg 1987)
3. I.W. Boyd: *Laser Processing of Thin Films and Microstructures*, Springer Ser. Mater. Sci., Vol. 3 (Springer, Berlin, Heidelberg 1987)
4. E. Fogarassy, S. Lazare (eds.): *Laser Ablation of Electronic Materials* (Elsevier, Amsterdam 1992)
5. D. Bäuerle, B. Luk'yanchuk, P. Schwab, X.Z. Wang, E. Arenholz: [4], p. 39
6. S.V. Babu, G.C. D' Couto, F.D. Egitto: *J. Appl. Phys.* **72**, 692 (1992) and references therein
7. J.H. Brannon, D. Scholl, E. Kay: *Appl. Phys. A* **52**, 160 (1991)
8. S. Küper, J. Brannon, K. Brannon: *Appl. Phys. A* **56**, 43 (1993)
9. A.H. Guenther, J.K. Mciver: *Thin Solid Films* **163**, 403 (1988)
10. D.L. Decker, L.G. Koshigoe, E.G. Ashley: *NBS Spec. Publ.* **727**, 291 (1986)
11. D. Ristau, X.C. Dang, J. Ebert: *NBS Spec. Publ.* **727**, 298 (1986)
12. S.M.J. Akhtar, D. Ristau, J. Ebert: *NIST Spec. Publ.* **752**, 345 (1988)
13. M.R. Lange, J.K. Mciver, A.H. Guenther: *Thin Solid Films* **125**, 143 (1985)
14. M.Z. Fuka, J.K. Mciver, A.H. Guenther: *NIST Spec. Publ.* **801**, 576 (1990)
15. J.M. Hicks, L.E. Urbach, E.W. Plummer, H.-L. Dai: *Phys. Rev. Lett.* **61**, 2588 (1988)
16. J.O. Porteus, D.L. Decker, W.N. Faith, D.J. Grandjean, S.C. Seitel, M.J. Soileau: *IEEE J. QE-17*, 2078 (1981)
17. Y. Jee, M.F. Becker, R.M. Walser: *J. Opt. Soc. Am. B* **5**, 648 (1988)
18. J.E. Andrew, P.E. Dyer, R.D. Greenough, P.H. Key: *Appl. Phys. Lett.* **43**, 1076 (1983)
19. S. Petzoldt, A.P. Elg, M. Reichling, J. Reif, E. Matthias: *Appl. Phys. Lett.* **53**, 2005 (1988)
20. A. Mandelis (ed.): *Principles and Perspectives of Photothermal and Photoacoustic Phenomena* (Elsevier, New York 1992)
21. D.L. Decker: *NIST Spec. Publ.* **752**, 89 (1988)
22. J.C. Lambropoulos, M.R. Jolly, C.A. Amsden, S.E. Gilman, M.J. Sinicropi, D. Diakomihalis, S.D. Jacobs: *J. Appl. Phys.* **66**, 4230 (1989)
23. R.T. Swimm: *SPIE* **1441**, 45 (1991)
24. J. Jauregui, E. Matthias: *Appl. Phys. A* **54**, 35 (1992)
25. O.W. Käding, E. Matthias, R. Zachai, H.-J. Füsler, P. Münzinger: *Diamond Relat. Mater.* **2**, 1185 (1993)
26. G. Busse, H.G. Walther: [20], Chap. 5, p. 205
27. H.J. Eichler, P. Günter, D.W. Pohl: *Laser-Induced Dynamic Gratings*, Springer Ser. Opt. Sci., Vol. 50 (Springer, Berlin, Heidelberg 1986)
28. O. Käding, E. Matthias: Unpublished
29. R.C. Weast (ed.): *Handbook of Chemistry and Physics*, 67th edn. (CRC, Boca Raton 1986–1987)